Hindawi
Journal of Nanomaterials
Volume 2019, Article ID 8346251, 7 pages
https://doi.org/10.1155/2019/8346251

Research Article

Controlled Synthesis of Porous Co_3O_4 Nanostructures for Efficient Electrochemical Sensing of Glucose

Jiankang Luo,[1] Jun Wu,[1] Zheng Liu,[2] Zenghe Li ,[1] and Li Deng [1,3]

[1]*College of Life Science and Technology, Beijing University of Chemical Technology, Beijing 100029, China*
[2]*Chinese Research Academy of Environmental Sciences, Beijing 100012, China*
[3]*Amoy-BUCT Industrial Bio-Technovation Institute, Beijing University of Chemical Technology, Amoy 361022, China*

Correspondence should be addressed to Zenghe Li; lizh@mail.buct.edu.cn and Li Deng; dengli@mail.buct.edu.cn

Received 20 May 2019; Accepted 10 August 2019; Published 16 September 2019

Guest Editor: Fei Ke

A shape-controlled strategy was developed to synthesize porous Co_3O_4 nanoparticles, and the delicate morphology including nanourchins, nanowires, nanoflowers, and nanoplates could be well adjusted by adopting different anion precursors. The Co_3O_4 nanomaterials were further applied as the electrocatalysts for glucose detection, and the effect of nanostructure on the electrochemical performance was investigated. Results show that Co_3O_4 nanourchins illustrate the highest glucose sensitivity of 565 mA mM^{-1} cm^{-2} and a good linear detection ranging from 20 μM to 0.25 mM. The improved performance of obtained products was originally from the large surface area and high pore volume, which leads to a significantly increased accessibility of reactant and decreased Faradic electron transfer resistance, making it a promising candidate for glucose sensing.

1. Introduction

In recent years, great efforts have been devoted to the development of highly sensitive and selective, cost-effective detectors for glucose in pharmaceuticals, food, and clinical diagnostics [1], due to their risk of increasing cholesterol content, food allergies, and diabetes. Among various methods, using an electrochemical sensor is recognized as one of the most promising techniques compared to its counterparts including optical [2], thermometric [3], and fluorescent [4] sensors, owing to its high sensitivity, reliability, and affordable cost. However, using conventional natural enzymes as a biological sensor suffers from several disadvantages for electrochemical glucose detection, such as high cost [5], storage difficulties, easy denaturation by environmental changes (e.g., temperature, humidity, and pH), and digestion by proteases [6]. Consequently, a series of nonenzymatic sensors have been proposed as the glucose probe in the past few decades, and these catalysts are mainly of noble metals (e.g., Au, Pt, and Pd), noble metal alloys (e.g., Pt–Pd, Pt–Cu, and Pt–Au), and transition metal oxides (e.g., Fe_3O_4, Co_3O_4, and CoO) [7]. However, the scarcity and high cost of these noble metal sensors make an obstacle for their applications, and it is still highly desired to develop alternative earth-abundant sensor materials with high efficiency [8].

Compared to noble metal-based glucose sensing catalysts, transition metal compounds are of low cost and abundant. Recent studies also show that shape-controlled synthesis of nanoparticles is capable of offering excellent performances in various applications [9–11]. Co_3O_4 is regarded as one of the most promising electrocatalysts for glucose detection. However, the inherently high electronic resistance and low surface area of Co_3O_4 retard its practical application [12]. Generally, the electrocatalytic properties of materials are strongly dependent on their morphology and microstructures, which creates substantial differences in the surface area, particle size, pore structure, mass transport, and electron transfer efficiency, which in turn influence their electrochemical sensing performance [13]. Therefore, the morphology and nanostructure control of Co_3O_4 are of vital importance to improve the electrochemical reactivity [6]. To this end, various Co_3O_4 nanoarchitectures such as nanospheres, nanocubes, and nanofibers have been synthesized by conventional precipitation, a hydrothermal process, and a

microwave-assisted approach [14]. Although there has been an extensive effort in the development of shape-controlled synthesis, the facile and mild approaches are still rare. Furthermore, few studies are focusing on the effect of morphologies and microstructures on the electrochemical activity of glucose detection [15].

Herein, a shaped-controlled synthesis route was developed to prepare Co_3O_4 nanostructures with tunable morphology by simply adopting different anions. The obtained Co_3O_4 nanourchins, nanowires, nanoflowers, and nanoplates are further used as the sensing materials for glucose detection, and the results reveal that Co_3O_4 nanourchins exhibit the highest glucose sensitivity of 565 mA mM^{-1} cm^{-2} and good stability due to the large surface area and low carrier transfer resistance [16].

2. Experiment

2.1. Synthesis of Co_3O_4 Nanomaterials. All chemicals were of analytical grade and used as received without further purification.

The porous Co_3O_4 nanostructures, including nanourchins, nanowires, nanoflowers, and nanoplates, were synthesized by a surfactant-assisted hydrothermal method using different cobalt precursors. Typically, 5 mM of $CoSO_4{\cdot}7H_2O$ or ($CoCl_2{\cdot}6H_2O$, $Co(NO_3)_2{\cdot}6H_2O$, and $Co(Ac)_2{\cdot}4H_2O$) was dissolved in water (40 mL) under stirring, followed by adding 1.5 g of $CO(NH_2)_2$ and 0.05 g of CTAB. After stirring for 30 min, the resulted transparent solution was transferred into a 50 mL autoclave, sealed, and maintained at 120°C for 12 h. After cooling to room temperature, the precipitate was collected by centrifugation, rinsed with water and ethanol, and dried at 80°C for 24 h. Finally, the obtained product was calcined at 500°C for 2 h in air.

2.2. Structural and Electrochemical Characterization of Co_3O_4 Nanomaterials. The composition and phase of the Co_3O_4 nanostructures were obtained by using the X-ray diffraction (XRD) profile on a Rigaku D/Max 2500 PC diffractometer with Cu Kα radiation ($\lambda = 1.54056$ Å) as the X-ray source. The morphology was examined by JEOL 6701F scanning electron microscopy (SEM). The N_2 adsorption-desorption analysis was measured on a Micromeritics Tristar 3020II instrument. Cyclic voltammetry (CV) and amperometry measurements were performed using a CHI660E electrochemical station (Chenhua, China) equipped with a standard three-electrode cell. The Co_3O_4 nanostructure-modified glassy carbon electrode (GCE) was used as the working electrode, while platinum wire and saturated calomel electrodes (SCE) served as the counter and reference electrodes, respectively. In preparing the working electrode, 5 mg of Co_3O_4 and 50 μL of Nafion (5 wt.%, DuPont) were ultrasonically dispersed in 1.0 mL ethanol for 0.5 h. Then, 6 μL of the homogeneous slurry was transferred onto the GCE (0.071 cm^2) and evaporated in an ambient atmosphere. The electrolyte was diluted with glucose in 0.1 M NaOH. Electrochemical impedance spectroscopy (EIS) measurements were performed at open-circuit potential with the frequency range of 0.1-100 kHz and an ac perturbation of 5.0 mV.

3. Results and Discussion

In our work, the porous Co_3O_4 nanostructures were synthesized using different cobalt precursors (see the experimental section in supporting information), and the morphology of the obtained products was firstly investigated and is shown in Figure 1. As observed, the featured morphologies of nanourchins, nanowires, nanoflowers, and nanoplates were realized by choosing distinct anion precursors. The self-assembly nanourchin Co_3O_4, which is obtained by using sulphate precursors, appears with an external diameter of about 3 μm, and the thorns grown on the surface are in the diameter of 23 nm with a length of 200 nm. Each urchin is estimated to have hundreds of thorns on the surface, which creates a significant roughness and offers a large surface area. Also, with all the thorns vertical to the surface, the transport would be facilitated if there were any reactions catalyzed over the nanostructure [17]. The chloridion-controlled Co_3O_4 synthesis, however, shows a significantly different structure of nanowires [18]. Each wire has a length of several micrometers and a diameter of 40 nm. The wire tends to aggregate with another or two, forming several combos, which reduces the surface area. With a careful examination, it can be seen that each wire is fabricated with about twenty nanorods end to end. This suggests that there has been a self-assembly process in the synthesis. The Co_3O_4 nanoflowers were prepared with the existence of nitrate ions. The flower has an apparent diameter of 15 μm and consists of dozens of twisted plates in the width of 0.6 μm and thickness of 0.1 μm. This self-assembled structure forms voids among the plates which is favorable to enlarge the surface area. However, compared to the nanourchin structure, the voids are confined between the plates, resulting in a poor interconnection [19]. The Co_3O_4 nanoplates were obtained with the presence of acetate. The plates are not that well-defined as those in the nanoflowers [20]. There are several random fragments and aggregates. The relatively large plates are in a width of 3 μm, and the thickness is about 0.1 μm.

The XRD patterns of the prepared Co_3O_4 nanomaterials are all indexed to a cubic Co_3O_4 phase, without any signal from other phases of cobalt oxides being detected, as shown in Figure 2. The higher intensity of the (311) plane as compared to the other planes could be observed from the patterns. In addition, the obvious broader peaks for Co_3O_4 nanourchins as compared to other nanostructures shown in Figure 2 (b–d) were observed, which is attributed to the suppression of crystal size by the sulphate anions. The grain sizes of the nanomaterials were estimated to be 16.9, 33.8, 22.5, and 28.1 nm for the Co_3O_4 nanourchins, nanowires, nanoflowers, and nanoplates, respectively, according to the Scherrer equation [21]. The variety in the grain size is believed to be caused by the tuned nucleation and grow process when different anions are present [22].

The surface area and pore structure of the Co_3O_4 nanomaterials were examined by the N_2 adsorption-desorption measurement. As shown in Fig. S1, each sample displays a type IV plot with a hysteresis loop. This suggests the presence of mesopores, which is confirmed by the Barrett-Joyner-Halenda (BJH) pore size distribution. The specific surface

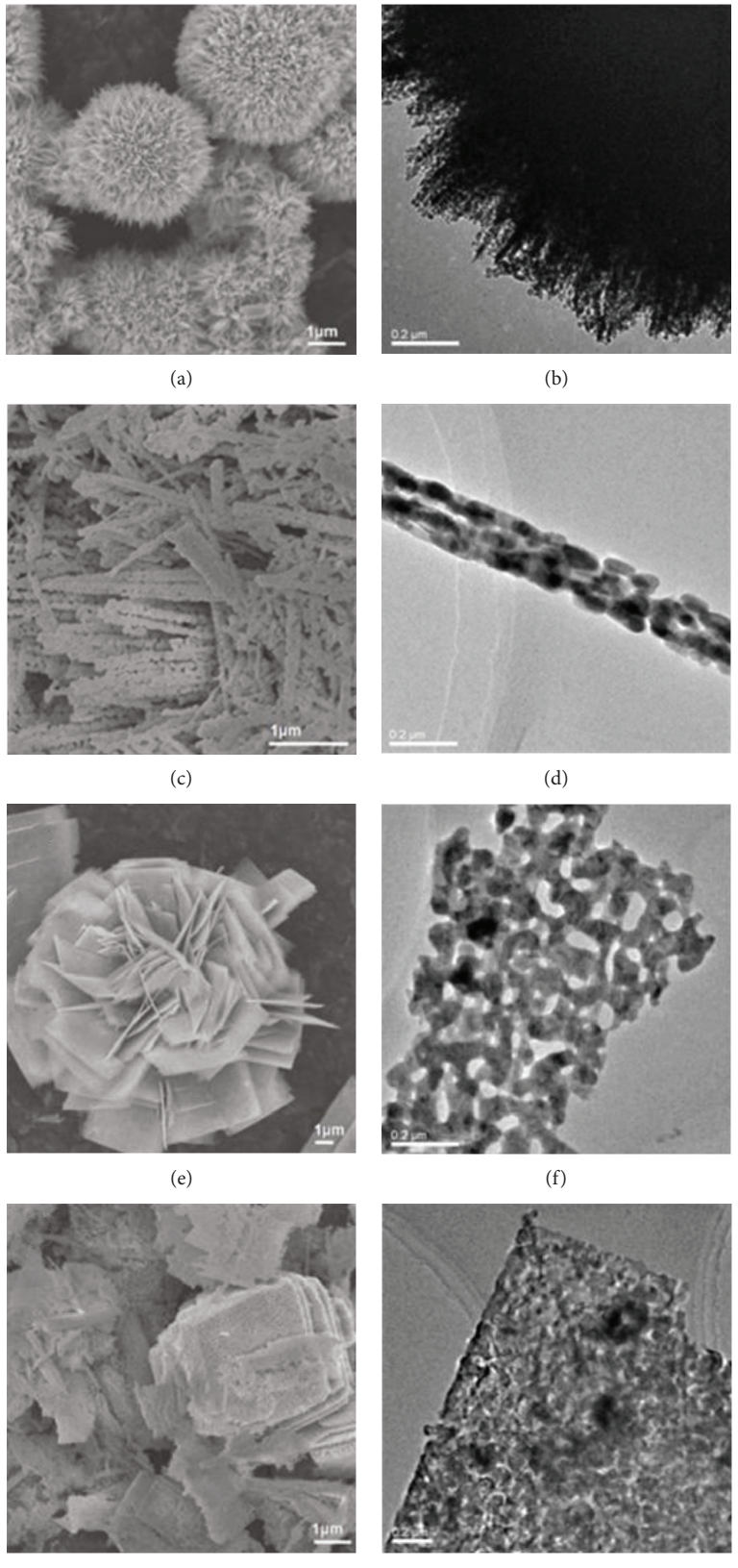

Figure 1: SEM and corresponding TEM images of Co_3O_4 synthesized with different anion precursors: (a, b) cobalt sulphate, (c, d) cobalt chloride, (e, f) cobalt nitrate, and (g, h) cobalt acetate.

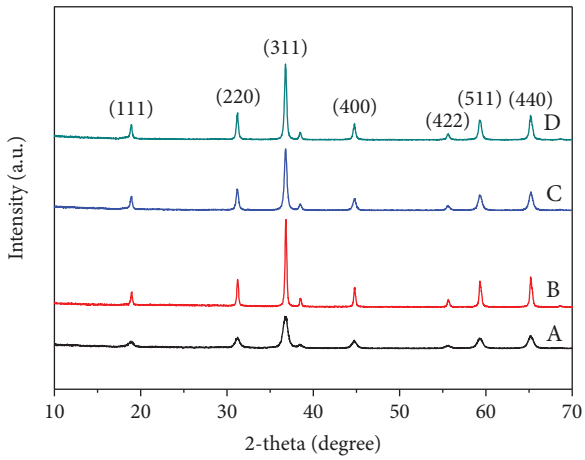

FIGURE 2: XRD patterns of the obtained Co_3O_4 nanoparticles after annealing treatment: (a) nanourchins, (b) nanowires, (c) nanoflowers, and (d) nanoplates.

area, pore volume, and average pore size of the Co_3O_4 nanomaterials are summarized in Table S1. The Co_3O_4 nanourchins have a specific surface area of 70.76 m^2 g^{-1}, which is significantly higher than that of the nanowires (11.75 m^2 g^{-1}), nanoflowers (9.93 m^2 g^{-1}), and nanoplates (13.06 m^2 g^{-1}). This feature is attributed to the abundant thorns with a small diameter of 23 nm grown on the surface of nanourchins. The average pore sizes of the Co_3O_4 nanourchins, nanowires, nanoflowers, and nanoplates are 10.81, 18.56, 36.22, and 36.27 nm, respectively, showing that the nanourchins have the smallest pores [23].

Further phase characterization of the Co_3O_4 nanomaterials before calcination was carried out to investigate the formation mechanism of the porous structure. As shown in Fig. S2, the uncalcined precursors have different phases. The peaks of the Co_3O_4 nanourchin precursor are composed of $CoCO_3$ (JCPDS: 11-0692) and $Co(OH)_2$ (JCPDS: 30-0443) [24]. While for a Co_3O_4 nanowire precursor, a pattern of $Co(CO_3)_{0.35}(Cl)_{0.20}(OH)_{1.10}{\cdot}1.74H_2O$ is discovered, the Co_3O_4 nanoflower precursor, however, is found to have the $Co(CO_3)_{0.5}(OH){\cdot}0.11H_2O$ (JCPDS: 48-0083) phase. As for the Co_3O_4 nanoplate precursor, a phase of $CoCO_3$ (JCPDS: 11-0692) is detected. These results suggest that the anions have a significant influence on the precursor formation due to the unique space-structure effect [25]. During heat treatment, the precursors decompose to oxide and release gas, which results in the formation of porous nanostructures [26].

The electrochemical activity towards glucose oxidation was determined by cyclic voltammetry (CV) and chronoamperometry. As shown in Figure 3, two pairs of redox peaks are observed for the Co_3O_4 nanomaterials in 0.1 M NaOH. The redox pair located between 0.1 and 0.4 V is attributed to the transformation of Co_3O_4/CoOOH, with the cathodic response which is not that obvious. The other redox pair of CoOOH/CoO_2 emerges between 0.5 and 0.6 V, as shown in

$$Co_3O_4 + OH^- + H_2O \rightarrow 3CoOOH + e^- \quad (1)$$

$$CoOOH + OH^- \rightarrow CoO_2 + H_2O + e^- \quad (2)$$

After the addition of 1 mM glucose, the peak currents of all the Co_3O_4 nanomaterials significantly increase due to the glucose oxidation. This electrochemical-chemical (EC) process is promoted by the Co_3O_4 intermediates, dominated by the CoO_2 species [27]. The glucose was oxidized by CoO_2 during the anodic scan and generated CoOOH. The formed CoOOH further contributes to the oxidation current, resulting in the increased anodic signal. The glucose detection by the Co_3O_4 nanomaterials is illustrated as follows [15].

$$CoOOH + OH^- \rightarrow CoO_2 + H_2O + e^- \quad (3)$$

$$CoO_2 + \text{glucose} \rightarrow CoOOH + \text{gluconolactone} \quad (4)$$

Therefore, the glucose oxidation activity of Co_3O_4 nanomaterials can be indicated by the increment in the anodic current density. With the addition of glucose, the current increase in Co_3O_4 nanourchins is 26.2 μA, which is higher than that with the Co_3O_4 nanowires (4.6 μA), nanoflowers (5.7 μA), and nanoplates (7.3 μA). The highest activity of Co_3O_4 nanourchins is attributed to the large surface area and facile accessibility of the active sites.

The Co_3O_4 nanomaterials were coated on the GCE and applied as the electrochemical sensor for glucose detection. As shown in Figure 4(a), the current increases when the glucose is added, suggesting the high electrochemical activity of Co_3O_4 nanomaterials [23, 28–30]. Figure 4(b) shows the linear relationship between the response current and the glucose concentration, and the sensitivity was calculated from the slope of the calibration curve [31]. It is observed that Co_3O_4 nanourchins have the highest electrochemical sensing performance, which is in agreement with the CV results. The detection limit is calculated to be 1.5 μM at a signal-to-noise ratio of 3 (S/N = 3) with a high sensitivity of 565 mA mM^{-1} cm^{-2} and a good linear detection ranging from 20 μM to 0.25 mM. The comparison between the previous reported glucose sensor and Co_3O_4 nanourchin-modified GCE is listed in Table S2. As can be seen, the Co_3O_4 nanourchin-modified GCE shows good performance towards the detection of glucose, offering a potential candidate for glucose detection application. Fig. S3 shows the EIS plots of Co_3O_4 nanomaterials at open-circuit potential in 0.1 M NaOH solution [28]. The plots consist of a well-defined semicircle in high frequency and a sloping line in low frequency [32]. The data was fitted to an equivalent circuit as shown in Fig. S3A, where Rs represents the inner resistance, Rct represents the Faradic electron transfer resistance, W is the Warburg impedance, Q_1 is the double-layer capacitance, and Q_2 is the pseudocapacitance [30]. The Faradic electron transfer resistance for the GCE modified by Co_3O_4 nanourchins, nanowires, nanoflowers, and nanoplates is 120, 421, 193, and 185 Ω, respectively. Notably, the Co_3O_4 nanourchin-modified GCE has the lowest Faradic electron transfer resistance, further confirming the highest electrochemical reactivity [15].

It is known that the possible coexisting species such as UA and AA may disturb the electrochemical detection of

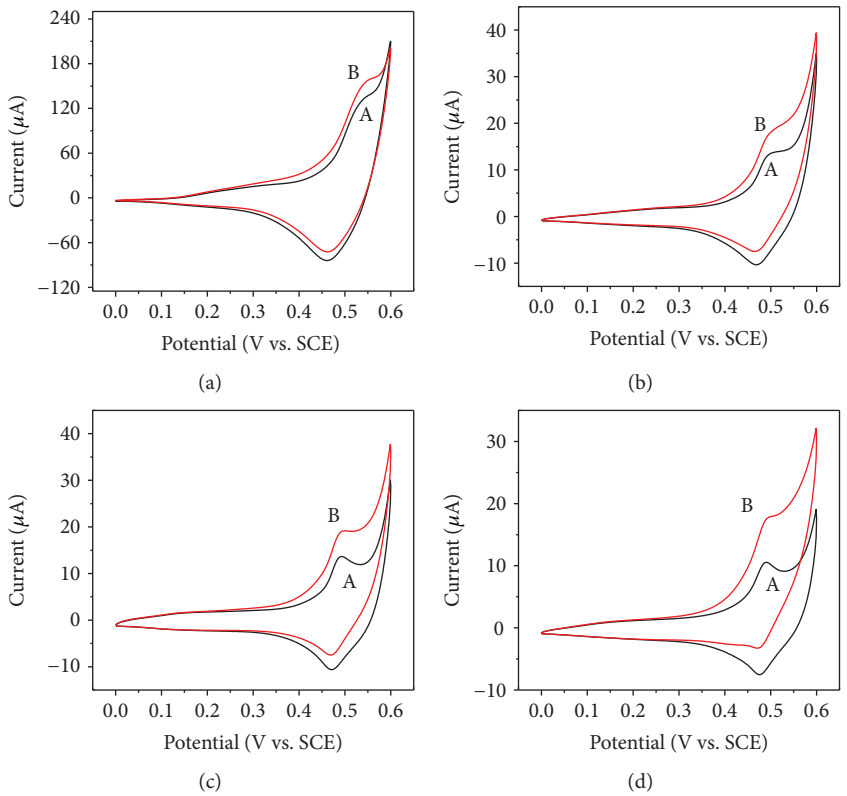

FIGURE 3: CV of Co_3O_4 (a) nanourchins, (b) nanowires, (c) nanoflowers, and (d) nanoplates (A) without and (B) with 1 mM glucose in 0.1 M NaOH.

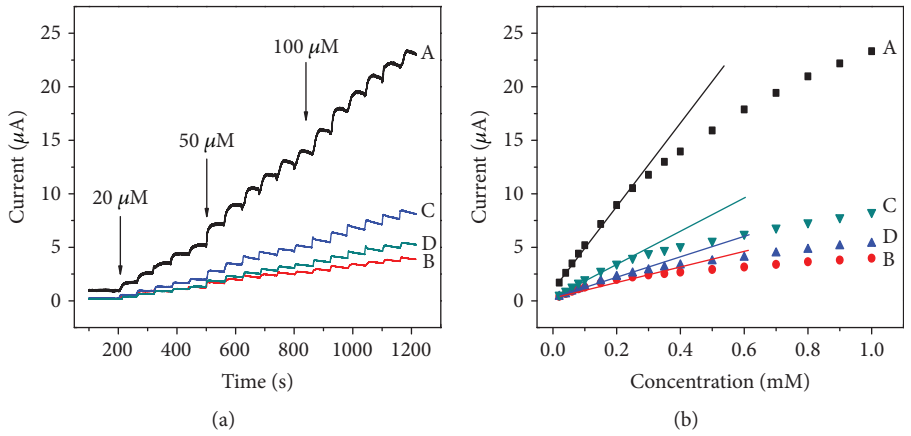

FIGURE 4: (a) Amperometric responses of Co_3O_4 (A) nanourchins, (B) nanowires, (C) nanoflowers, and (D) nanoplates. (b) Linear relationship between the response current and glucose concentration.

glucose. Fig. S4 shows the glucose selectivity of the Co_3O_4 nanourchin-modified GCE when adding UA and AA. The response current increases remarkably with the addition of glucose, but it remained almost unchanged when the UA or AA was dropped in [33]. Therefore, the Co_3O_4 nanourchin-modified electrode has a good selectivity towards glucose.

As for the reproducibility and stability, five individual tests were measured using the Co_3O_4 nanourchin-modified electrode [29]. Results show that the relative standard deviation (RSD) was only 2.9% when detecting 50 μM glucose. When the electrode was stored at 4°C for two weeks, the amperometric current only declined by 2.4%. Therefore, the Co_3O_4 nanourchin-modified electrode is stable with excellent reproducibility, which is very favorable for practical application [34–36].

4. Conclusions

In summary, a facile hydrothermal strategy was applied to synthesize porous Co_3O_4 with various morphologies. The effect of morphology and microstructures on the electrochemical performance was investigated, and the results show

that the Co_3O_4 nanourchins are self-assembled by hundreds of thorns with a three-dimensional porous network, which offer a higher surface area of 70.76 m^2 g^{-1} compared with that of Co_3O_4 nanowires, nanoflowers, and nanoplates. Electrochemical measurements reveal that the glucose sensor based on a Co_3O_4 nanourchin electrode demonstrates the significantly highest sensing performance with a high sensitivity of 565 $\mu A\,mM^{-1}$ cm^{-2} and a linear detection range of 20-250 μM as well as a low detection limit of 1.5 μM. The superior sensing performance is attributed to the higher specific surface area with a three-dimensional porous network and the lower Faradic electron transfer resistance of the urchin-like Co_3O_4. Therefore, this unique urchin-like Co_3O_4 is a promising candidate as a glucose sensor.

Data Availability

The data used to support the findings of this study are included within the article.

Conflicts of Interest

The authors declare that there is no conflict of interests regarding the publication of this paper.

Acknowledgments

This work was supported by the National Key Research Development Program (Grant No. 2016YFD0400601).

Supplementary Materials

Figure S1: nitrogen adsorption/desorption isotherms and corresponding BJH pore size distribution (inset) of Co_3O_4 (a) nanourchins, (b) nanowires, (c) nanoflowers, and (d) nanoplates. Table S1: the surface area, pore volume, and average pore size of Co_3O_4 nanomaterials. Figure S2: the XRD patterns of obtained Co3O4 nanoparticles before annealing treatment: (a) nanourchins, (b) nanowires, (c) nanoflowers, and (d) nanoplates. Table S2: performances of typical electrochemical sensing materials for glucose detection. Figure S3: impedance Nyquist plots of Co_3O_4 (a) nanourchins, (b) nanowires, (c) nanoflowers, and (d) nanoplates at open-circuit potential in 0.1 M NaOH solution. Figure S4: the amperometric response to the addition of glucose with interfering species. *(Supplementary Materials)*

References

[1] J.-L. Ma, B.-C. Yin, X. Wu, and B.-C. Ye, "Simple and cost-effective glucose detection based on carbon nanodots supported on silver nanoparticles," *Analytical Chemistry*, vol. 89, no. 2, pp. 1323–1328, 2016.

[2] J. He, X. Lu, J. Yu, L. Wang, and Y. Song, "Hierarchical $Co(OH)_2$ nanostructures/glassy carbon electrode derived from Co(BTC) metal–organic frameworks for glucose sensing," *Journal of Nanoparticle Research*, vol. 18, no. 7, pp. 184–195, 2016.

[3] X. Y. Yu, Z. G. Liu, and X. J. Huang, "Nanostructured metal oxides/hydroxides-based electrochemical sensor for monitoring environmental micropollutants," *Trends in Environmental Analytical Chemistry*, vol. 3-4, pp. 28–35, 2014.

[4] G. Rajeshkhanna, E. Umeshbabu, and G. Ranga Rao, "Charge storage, electrocatalytic and sensing activities of nest-like nanostructured Co_3O_4," *Journal of Colloid and Interface Science*, vol. 487, pp. 20–30, 2017.

[5] P. Sivasakthi, G. N. K. Ramesh Bapu, and M. Chandrasekaran, "Pulse electrodeposited nickel-indium tin oxide nanocomposite as an electrocatalyst for non-enzymatic glucose sensing," *Materials Science and Engineering: C*, vol. 58, pp. 782–789, 2016.

[6] S. Park, H. Boo, and T. D. Chung, "Electrochemical non-enzymatic glucose sensors," *Analytica Chimica Acta*, vol. 556, no. 1, pp. 46–57, 2006.

[7] Y. Li, C. Zhong, J. Liu et al., "Atomically thin mesoporous Co_3O_4 layers strongly coupled with N-rGO nanosheets as high-performance bifunctional catalysts for 1D knittable zinc–air batteries," *Advanced Materials*, vol. 30, no. 4, article 1703657, 2018.

[8] Z. Cai, Y. Bi, E. Hu et al., "Single-crystalline ultrathin Co_3O_4 nanosheets with massive vacancy defects for enhanced electrocatalysis," *Advanced Energy Materials*, vol. 8, no. 3, pp. 1–8, 2018.

[9] P. Hu, Z. Jia, H. Che et al., "Engineering hybrid $CoMoS_4/Ni_3S_2$ nanostructures as efficient bifunctional electrocatalyst for overall water splitting," *Journal of Power Sources*, vol. 416, pp. 95–103, 2019.

[10] X. Yan, Z. Jia, H. Che et al., "A selective ion replacement strategy for the synthesis of copper doped carbon nitride nanotubes with improved photocatalytic hydrogen evolution," *Applied Catalysis B: Environmental*, vol. 234, pp. 19–25, 2018.

[11] H. B. Che, X. X. Yan, Z. Y. Jia, P. Hu, and J. S. Wang, "Phosphorus doped carbon nitride nanotubes by sequential cation-exchanging reaction with enhanced photocatalytic hydrogen evolution," *Journal of Nano Research*, vol. 53, pp. 76–85, 2018.

[12] Z. Wang, H. Liu, R. Ge et al., "Phosphorus-doped Co_3O_4 nanowire array: a highly efficient bifunctional electrocatalyst for overall water splitting," *ACS Catalysis*, vol. 8, no. 3, pp. 2236–2241, 2018.

[13] W. Li, D. Liu, X. Feng, Z. Zhang, X. Jin, and Y. Zhang, "High-performance ultrathin Co_3O_4 nanosheet supported PdO/CeO_2 catalysts for methane combustion," *Advanced Energy Materials*, vol. 9, no. 18, article 1803583, 2019.

[14] J. Xu, F. Li, D. Wang et al., "Co_3O_4 nanostructures on flexible carbon cloth for crystal plane effect of nonenzymatic electrocatalysis for glucose," *Biosensors and Bioelectronics*, vol. 123, pp. 25–29, 2019.

[15] L. Tian, G. He, Y. Cai et al., "Co_3O_4 based non-enzymatic glucose sensor with high sensitivity and reliable stability derived from hollow hierarchical architecture," *Nanotechnology*, vol. 29, no. 7, pp. 75502–75506, 2018.

[16] M. H. Yang, J.-M. Jeong, K. G. Lee, D. H. Kim, S. J. Lee, and B. G. Choi, "Hierarchical porous microspheres of the Co_3O_4@ graphene with enhanced electrocatalytic performance for electrochemical biosensors," *Biosensors and Bioelectronics*, vol. 89, Part 1, pp. 612–619, 2017.

[17] P. Hu, C. K. Ngaw, Y. Yuan, P. S. Bassi, S. C. Joachim Loo, and T. T. Yang Tan, "Bandgap engineering of ternary sulfide nanocrystals by solution proton alloying for efficient photocatalytic H_2 evolution," *Nano Energy*, vol. 26, pp. 577–585, 2016.

[18] T. Liu, L. Zhang, W. You, and J. Yu, "Core–shell nitrogen-doped carbon hollow spheres/Co_3O_4 nanosheets as advanced electrode for high-performance supercapacitor," *Small*, vol. 14, no. 12, pp. 1–6, 2018.

[19] P. Tan, B. Chen, H. Xu, W. Cai, W. He, and M. Ni, "Porous Co_3O_4 nanoplates as the active material for rechargeable Zn-air batteries with high energy efficiency and cycling stability," *Energy*, vol. 166, pp. 1241–1248, 2019.

[20] P. Tan, Z. Wu, B. Chen, H. Xu, W. Cai, and M. Ni, "Exploring oxygen electrocatalytic activity and pseudocapacitive behavior of Co_3O_4 nanoplates in alkaline solutions," *Electrochimica Acta*, vol. 310, pp. 86–95, 2019.

[21] K. Fukui and Y. Suzuki, "Well-facetted spinel-type Co_3O_4 microcrystal assembly prepared by hydrothermal synthesis and post-thermal decomposition," *Ceramics International*, vol. 45, no. 7, pp. 9288–9292, 2019.

[22] G. Anandhababu and G. Ravi, "Facile synthesis of quantum sized Co_3O_4 nanostructures and their magnetic properties," *Nano-Structures & Nano-Objects*, vol. 15, pp. 1–9, 2018.

[23] Y. Jiang, X. Yan, P. Mei, Y. Zhang, W. Xiao, and H. Tang, "Electrochemical reconstruction induced high electrochemical performance of Co_3O_4/reduced graphene oxide for lithium ion batteries," *Journal of Alloys and Compounds*, vol. 764, pp. 80–87, 2018.

[24] Z. Huang, Y. Zhao, H. Xu, and J. Zhao, "Surfactant-free synthesis, photocatalytic and electrochemical property study of Co_3O_4 nanoparticles," *Materials Research Bulletin*, vol. 100, pp. 83–90, 2018.

[25] M. Y. Nassar, "Size-controlled synthesis of $CoCO_3$ and Co_3O_4 nanoparticles by free-surfactant hydrothermal method," *Materials Letters*, vol. 94, pp. 112–115, 2013.

[26] Z. Ding, B. Yao, J. Feng, and J. Zhang, "Enhanced rate performance and cycling stability of a $CoCO_3$–polypyrrole composite for lithium ion battery anodes," *Journal of Materials Chemistry A*, vol. 1, no. 37, pp. 11200–11209, 2013.

[27] X. Peng, H. X. Li, H. J. Shao et al., "Involvement of calcium-sensing receptors in hypoxia-induced vascular remodeling and pulmonary hypertension by promoting phenotypic modulation of small pulmonary arteries," *Molecular and Cellular Biochemistry*, vol. 396, no. 1-2, pp. 87–98, 2014.

[28] X. Xiao, X. Liu, H. Zhao et al., "Facile shape control of Co_3O_4 and the effect of the crystal plane on electrochemical performance," *Advanced Materials*, vol. 24, no. 42, pp. 5762–5766, 2012.

[29] Y. Liang, Y. Li, H. Wang et al., "Co_3O_4 nanocrystals on graphene as a synergistic catalyst for oxygen reduction reaction," *Nature Materials*, vol. 10, no. 10, pp. 780–786, 2011.

[30] Y. P. Zhu, T. Y. Ma, M. Jaroniec, and S. Z. Qiao, "Self-templating synthesis of hollow Co_3O_4 microtube arrays for highly efficient water electrolysis," *Angewandte Chemie International Edition*, vol. 56, no. 5, pp. 1324–1328, 2017.

[31] J. Mu, L. Zhang, M. Zhao, and Y. Wang, "Catalase mimic property of Co_3O_4 nanomaterials with different morphology and its application as a calcium sensor," *ACS Applied Materials & Interfaces*, vol. 6, no. 10, pp. 7090–7098, 2014.

[32] J. E. Kessler, A. Aliaga, N. Rosales Espitia, C. Rugge, and N. Myung, "Controlled synthesis of electrocatalytic Co_3O_4 nanofibers via electrospinning," vol. 8, pp. 324–328, 2016.

[33] T. Zhai, L. Wan, S. Sun et al., "Phosphate ion functionalized Co_3O_4 ultrathin nanosheets with greatly improved surface reactivity for high performance pseudocapacitors," *Advanced Materials*, vol. 29, no. 7, pp. 160–167, 2017.

[34] J. Ma, S. Zhang, W. Liu, and Y. Zhao, "Facile preparation of Co_3O_4 nanocrystals via a solvothermal process directly from common Co_2O_3 powder," *Journal of Alloys and Compounds*, vol. 490, no. 1-2, pp. 647–651, 2010.

[35] K. Tian, K. Baskaran, and A. Tiwari, "Nonenzymatic glucose sensing using metal oxides–comparison of CuO, Co_3O_4, and NiO," *Vacuum*, vol. 155, pp. 696–701, 2018.

[36] E. Zhang, Y. Xie, S. Ci, J. Jia, and Z. Wen, "Porous Co_3O_4 hollow nanododecahedra for nonenzymatic glucose biosensor and biofuel cell," *Biosensors and Bioelectronics*, vol. 81, pp. 46–53, 2016.